Post-Buckled Composite Panels for Helicopter Fuselages: Design, Analysis, Fabrication and Testing

Donald J. Baker*
Vehicle Technology Directorate - ARL
NASA Langley Research Center
Hampton, VA 23681

Christos Kassapoglou
Sikorsky Aircraft
MS S-352A
6900 Main Street
Stratford, CT 06615

Abstract

For the lightly-loaded structures (200 lbs/in. in compression and 400 lbs/in. in shear), the traditional skin-stiffened structure is more efficient than sandwich structure due to the minimum gage requirements imposed on the sandwich structure. A design for minimum weight and cost T-stiffened panel that was designed for a 120 lbs/in. compression load and 337 lbs./in. shear loading condition is presented. The finite element analysis and testing of the T-stiffened structural concept is presented. The results of a nonlinear finite element analysis for a perfect panel and a panel that included manufacturing imperfections is presented. Two panels have been tested in compression to 200 lbs/in., a post-buckling load factor of nearly two, without failure. The axial prebuckled stiffness of the test panels was 15 to 40 percent higher than the predicted stiffness. The same panels were tested in shear to approximately 400 lbs/in. without failure. The analysis predicted the shear buckling load to be within 10% of the test results. A comparison between the analysis and the experimental results is presented.

Introduction

Use of composites in helicopter primary structures has been steadily increasing over the past two decades. A prime example is the RAH-66 Comanche fuselage, which consists mostly of sandwich construction for the skins, frames, bulkheads, keel beams, decks and doors. Sandwich composite panels are very efficient for non-buckling structural designs because of the increased bending stiffness, which allows each panel to carry both shear and compression loads. However, for relatively lightly loaded structures (compression below 200 lbs/in. and shear below 400 lbs/in.) the sandwich design becomes inefficient because of minimum gage requirements. For sandwich construction the core thickness is limited to no less than 0.25 inches and the facesheet thickness is limited to no less than 0.015 inches in order to avoid moisture absorption problems. The applied loads are such that designs with lower facesheet and core thicknesses than above would be adequate but cannot be used. Alternate designs are needed that may be more efficient in this load regime.

One of the alternate design concepts that is under investigation in the US Army/Sikorsky Rotary Wing Structures Technology Demonstration program, is the traditional skin-stiffened panel that is allowed to post-buckle at a high enough post-buckling factor that could compete with the buckling resistant design. Post-buckling factor is defined as the ratio of the applied load to the buckling load. This may require post-buckling factors significantly higher than 1.5, which makes the structure very susceptible to damage initiation and growth during fatigue loading since the structure buckles below limit load. This can be a major concern especially for structures exposed to driving frequencies from the main or tail rotor.

As a first step towards investigating the potential of postbuckled skin-stiffened panels loaded in low-level compression and shear loads, the static design, analysis and testing of such a panel was undertaken in this study. Typical dimensions and loads for a composite helicopter fuselage were assumed. The square shaped panel was assumed with

* Senior Aerospace Engineer

Presented at the American Helicopter Society Hampton Roads Chapter, Structure Specialists Meeting Williamsburg, VA, Oct 30 – Nov 1, 2001

a side dimension of 21 inches, and the applied (ultimate) loads were 120 lbs/in. in compression and 337 lbs/in. in shear. A typical toughened graphite-epoxy material in the tape and fabric form was used for making the stiffened panel.

This paper will present the design, fabrication, finite element analysis and testing of a lightly-loaded stiffened panel. For simplicity the panels were loaded first in compression to a predetermined load. After compression testing the panels were then modified to fit an existing picture frame test fixture and tested in shear. An analysis was conducted for each test condition to predict the buckling and postbuckling response.

Panel Design

The panel design was based on results from reference [1] where postbuckled stiffened composite panels with stiffeners of various cross-sections were optimized simultaneously for cost and weight. It was found in reference [1] that the best stiffener shapes were (in order of decreasing efficiency): L, C, Z, T, J, and Hat. However, due to the concerns mentioned earlier related to fatigue loading, candidate cross-sections that have an exposed radius region at the stiffener base, such as the L, C, and Z stiffener were eliminated. Under fatigue loads, microcracks would develop in the resin pocket that forms during fabrication at the skin-stiffener juncture right below the stiffener web. These microcracks may lead to delaminations and premature failure. As a result, the T-stiffener configuration was selected for the design. The stiffener dimensions and layup selections are shown in Figure 1. The skin layup was assumed to be quasi-isotropic and made up of plain weave fabric material. The skin thickness and the stiffener spacing were treated as variables. The procedure to determine the stiffener spacing and skin stiffness followed the analysis and Pareto optimization approach described in reference [1].

The stiffener spacing was varied successively from 2 to 8 inches and, for each case, the optimum skin thickness for minimum weight and cost were determined, treating the skin thickness as a continuous variable. The postbuckling factor was set to 3 and the panel was designed not to have skin tearing failure or stiffener crippling and buckling failures under the applied loads. The results are shown in Figure 2 where the optimum cost is plotted against the optimum weight (as the skin thickness varies). It should be noted that the cost value is referred to as "typical" since it is not representative of actual factory practices. However, the relative differences in cost between designs can be considered as representative of actual trends.

Discontinuities in the curve of Figure 2 correspond to cases where the stiffener spacing increases enough so that an entire stiffener is eliminated from the design. As is seen in Figure 2, the minimum weight design corresponds to a very different configuration than the design for minimum cost. To determine the overall cost and weight minimum, the approach in reference [1] was used. The cost and weight data in Figure 2 were normalized by the minimum corresponding values and the quantity

$$\text{Figure of Merit (FM)} = [(\text{Wt}-\text{Wt}_{\text{min}})^2/(\text{Wt}_{\text{min}})^2 + (\text{Cost}-\text{Cost}_{\text{min}})^2/(\text{Cost}_{\text{min}})^2]^{1/2}$$

was computed which is the minimum radial distance to the normalized cost versus normalized weight curve (see reference [1]). This quantity (FM) is plotted in Figure 3 as a function of stiffener spacing.

The point where the figure of merit is minimized (where the radial distance of a design point to the origin in normalized cost/weight space is minimized) corresponds to the design that minimizes cost and weight if the cost and weight are given equal importance by the designer. As is seen from Figure 3, this corresponds to a stiffener spacing that is slightly larger than 4 inches. For purposes of this investigation, the stiffener spacing was chosen to be 4 inches, and the skin thickness was chosen at 0.03 inches, corresponding to the value generated by the optimizer.

Fabrication

The two stiffened panels were hand laid up using plain weave materials for the skin and combinations of plain weave fabric and unidirectional tape for the stiffeners (see Figure 1). The material system used was IM7/8552 graphite-epoxy. Each of the two halves of the five T-stiffeners was hand laid on separate male mandrels. The mandrels had a triangular cross-section with a 0.125-inch radius at the vertex of the 90-degree angle to define the stiffener corner radius. The mandrel side opposing the right angle was at 45 degrees to ensure good pressure transfer on both the web and flange of each stiffener during cure (see Figure 4). Each of the two halves of the stiffeners was located on the flat aluminum plate where the $[-45^f/0_2^f/45^f]$ skin of 0.0075-in. thick fabric had already been laid up. A 0.5-in-wide by 21-in.-long piece of unidirectional tape was rolled and located at the bottom of the web

of each stiffener to act as a filler. The entire assembly was bagged and cured following the recommended material cure cycle. A photograph of the as-fabricated panel is shown in Figure 5. The final weight of each panel was 1.15 pounds.

Test Panel Analysis

Analysis Procedure

The panel considered in this study was analyzed using STAGS (STructural Analysis of General Shells) nonlinear shell finite element analysis computer code (reference [2]). STAGS is a code for the static and dynamic analysis of general shells, and includes the effects of geometric and material nonlinearities in the analysis. The code uses both the modified and full Newton methods for its nonlinear solution algorithms, and accounts for large rotation in a shell by using a co-rotational algorithm at the element level. The Riks pseudo arc-length path-following method (reference [3]) is used to continue a solution past the limit points of a nonlinear response. With this strategy, the incrementally applied loading parameter is replaced by an arc-length along the solution path, which is then used as an independent loading parameter. The arc length increment is automatically adjusted by the program as a function of the solution behavior. The code also contains a solution branch switching algorithm that offers the user the opportunity to jump from one solution path to another in the vicinity of a bifurcation point. The transient analysis option in STAGS uses proportional structural damping and an implicit numerical time-integration method developed by Park (reference [4]).

Modeling and Analysis of Compression Test Panel

A finite element model (model 1) of the 21-inch square I-stiffened panel is illustrated in Figure 6. The standard 4-node quadrilateral element from the STAGS element library (element 410) was used to model the panel. The elements are approximately 0.25-in. square. The model contains 8925 nodes and 8736 quadrilateral elements. The unidirectional carbon-epoxy filler (Figure 4) was modeled as beams. This added 420 beams to the model for a total of 9156 elements. A geometrically perfect panel was analyzed using this model. Nominal panel geometry, laminate thickness and material properties shown in Table 1 were used in the finite element model for the panel. The boundary conditions used in the analysis are shown in Figure 7. These boundary conditions model the end potting as a rigid material. The panel was loaded in axial compression at 120 lbs/in., which is the design ultimate load.

A linear analysis was performed on the panel at the design ultimate load and the predicted v and w displacements are shown in Figure 8. The predicted panel end shortening corresponding to the ultimate load was 0.0089 inches. This gives a predicted axial stiffness of 283,146 lbs/in. A linear eigenvalue analysis predicted the initial buckling load at 117.5 lbs/in., which is 98 percent of the applied load. The predicted mode shapes and the critical loads for the first four modes are shown in Figure 9. Note modes 1 and 2 shown in Figure 9 are very similar, and so are modes 3 and 4. The stiffener at this stiffener-skin junction remains straight in the predicted buckled mode shape, thereby acting as panel breakers for the 4-ply skin while the stiffener leg indicates some roll.

A second finite element model, model 2, was generated where the element size was approximately twice the element size used in model 1. This model has 2537 nodes and 2647 elements, which include 211 beam elements and is intended to reduce the computational time. The boundary conditions here were the same as for model 1 except that the conditions at y = 0.25 and 20.75 were not needed with the larger element size. A linear static analysis was performed on the panel at the design ultimate load with the resulting predicted w displacement shown in Figure 10. The panel end shortening was 0.0080 in. which is 90 percent of the end shortening predicted using model 1. This linear analysis predicts an axial stiffness of 315,000 lbs/in. As shown in Figure 10, the skin in each bay deflects in the same direction, which is the same as in model 1. A linear eigenvalue analysis predicted the initial buckling load at 141.2 lbs/in. Note that this initial buckling load is 118 percent of the applied load. The predicted mode shapes and the critical loads for the first four modes are shown in Figure 11. The predicted mode shapes from model 2 (Figure 11) appear reversed from model 1 mode shapes (Figure 9). This is not surprising for this eigenvalue problem and so are the very small differences between modes 1 and 2 or modes 3 and 4.

A nonlinear analysis was performed using model 2 to a load of approximately 300 lbs/in. The initial imperfection introduced to start the nonlinear analysis was the summation of 0.03 times the first and second mode shapes. The predicted first buckling mode with a nonlinear prestress is 165.2 lbs/in. The predicted panel end shortening as a nonlinear function of load is shown in Figure 12. The predicted end shortening from the nonlinear

analysis is 0.0084 inches at ultimate load. The calculated panel initial axial stiffness is 300,000 lbs/in. Predicted deformed shapes for the panel are shown in Figure 13 for selected load levels up to 300 lbs/in. The analysis indicated that the skin in each bay deforms out-of-plane starting with the initial loading. As shown in Figure 13, the displacements in each bay occur with an appearance of a half-wave near each loaded edge of the panel with an oblong shaped deformation at the center of each stiffener bay and deflecting in the direction opposite to that at the ends. As the load increases the oblong shape develops into two half-waves in adjacent stiffener bays. The displacement directions change direction in adjacent bays suggesting that the stiffeners effectively act as nodal line. By the time the load increases to N_y = 166 lbs/in., the center oblong displacement appears as adjacent half waves displacing in the same direction. The positive and negative magnitudes of the deflections are approximately the same from the plane of the skin until the load approaches 300 lbs/in., where the negative displacement is greater than the positive displacement. This change in magnitude is shown in the profile of the w displacements along the length of the panel at a distance 8.12 inches away from the corner (near center of second skin bay) in Figure 14 for applied loads of N_y = 166 lbs/in and N_y = 300 lbs/in. Figure 14 indicates that as the load increases, the deflection at the center of the bay increases in the negative direction while at the end of the bay there is only a small increase in deflection in the positive direction. This is an indication of transition from a local to global buckling mode.

Model 3 is a modification of model 2 and incorporates the measured manufacturing geometric imperfections in the flatness of the skin into the finite element model. A surface was fit to the measured geometric data for panel #2 with the resultant surface geometry shown in Figure 15. The panel imperfection varies from +0.047-inches to –0.172-inches from a plane determined by three points on the panel. This deformed geometry was incorporated into model 3. The stiffeners were also modeled as deformed in the z direction, thus keeping a constant stiffener height. The same element size and boundary conditions as in model 2 were used in this model. The ultimate load of 120 lbs/in. was applied.

A linear eigenvalue analysis using model 3 predicted a buckling load of 121.8 lbs/in. The mode shapes are the same as those obtained from the linear analysis of a geometrically perfect panel model (Figure 11). The linear analysis predicted a panel end shortening of 0.009 inches, which corresponds to an axial stiffness of 280,000 lbs/in. The predicted linear out-of-plane displacement contours and magnitudes are different from those obtained from the ideal models and are shown in Figure 16. The maximum displacements are in the center of the stiffener bay rather than at the end of the bays as shown in Figure 10. The two outside bays have a larger displacement than the two center bays. A nonlinear analysis was performed to a loading of approximately 250 lbs/in. The predicted out-of-plane displacements for selected applied loads are shown in Figure 17. The predicted initial axial stiffness is 264,800 lbs/in. from the nonlinear analysis. A comparison of Figure 17 with Figure 13 indicates that this displacement pattern is different than that for the perfect panel models. The predicted out-of-plane displacement contours are in the form of four half-waves in each stiffener bay. The w displacement at the end of each bay is in opposite directions while the ideal models displacements are in the same direction. At low loads each bay has four half-waves while the perfect panel models have a half-wave at each end with a long wave in between. At loads less than 220 lbs/in. the out-of-plane deflections are approximately the same in each direction, but as loads increase the deflection in the negative direction increases faster than the deflection in the positive direction. As the loads increase past approximately 230 lbs/in. one of the half-waves in each bay begins to change into two half waves.

Modeling and analysis of shear test panel

To use an existing shear testing fixture that has a 17-inch square test area it was necessary to modify the finite element model of the stiffened panel. Model 2 from the compression analysis was modified by reducing its size to 17-inches square and the web of each outside stiffener was removed to provide clearance for the test fixture which resulted in three T-stiffeners. The increased thickness from the stiffener flanges of the outside stiffeners remained on the panel and in the model. The resulting model is shown in Figure 18. By the use of Lagrange (multi-point) constraints in STAGS, the model was forced to deform from a square to a parallelogram as shown in Figure 19. This is a reasonable assumption since the fixture is considered very stiff when compared to the panel, but this assumption does not consider the effects of the pivot pin locations in the shear fixture.

A linear eigenvalue analysis predicted buckling at 81.8 lbs/in. in shear. The predicted mode shapes for the panel are shown in Figure 20. Mode 2 eigenvalue is the reverse of mode 1 value. A nonlinear analysis was performed to a load of approximately 500 lbs/in. with selected results shown in Figure 21. An initial imperfection that is 0.005

times the first mode shape was used in the analysis. From the predicted shapes shown in Figure 21 it can be seen that the deflections increase in depth as the load increases and more buckles move in from the diagonally opposite corners. The displacement at Points A and B (Figure 19) are shown in Figure 22. The linear analysis for the deflection of Point B is also shown in Figure 22 for comparison. It can be seen in Figure 22 that the mode shape changes at approximately 150 lbs/in. with a change in the direction of deflection at Point A, another change occurs at approximately 250 lbs/in.

Test Results and Comparison with Analysis Results

The 5-stringer panels with designations EWR-104079-B and EWR-104079A will be identified as Panel #1 and Panel #2, respectively, for this paper. Each end of the panel was potted with a filled epoxy to a depth of 0.5-inches and machined flat and parallel to an overall length of 20-inches or 21-inches. A fabrication defect required cutting one panel to a 20-inch length. Knife edge supports were used to support the panel side edges for the compression tests. Twenty eight strain gages were installed on each panel as shown in Figure 23. Six LVDT's were used in the test setup to determine panel end-shortening and out-of-plane displacements. All specimen tests were performed at room temperature in the as-fabricated condition. The specimens were placed between the platens of a 120-kip hydraulic test machine and loaded in compression at a rate of less than 1,000 lbs/min. to a load of 4,200 lbs (200 lbs/in.) and then unloaded. A video camera and a still camera were used to record changes in the moiré fringe pattern during the tests. The load, strain, out-of-plane and loading head displacements were recorded with a computer-controlled data acquisition system for each test. The experimental results for each panel are compared with analytical results below.

Compression Loading

Panel #1 - The strain results from the 28 gages on Panel #1 are shown in Figures 24 and 25. The strains corresponding to a complete load and unload cycle are shown in these figures. The dashed lines in Figures 24 are the results from the gage on the flat or skin side. The dashed line in Figures 25 indicated the results from the high gage numbers in each pair of back-to-back gages. The minor offset in the curves at approximately 160 lbs/in. is suspected to be a test machine induced anomaly (i.e., when the machine transitions from supporting the upper loading head to applying a load through it). Note that the experimental strain results shown in Figure 24 are very low, less than 0.0005 in/in., and do not indicate that buckling occurred in the skin and are nearly linear up to the maximum load. The predicted skin surface strains from model 2 nonlinear analysis are also shown in Figure 24 as curves with a triangle or circle symbol at the end. There is good correlation between experimental strains and analysis up to approximately 75 lbs/in., at which time the predicted strains in the bay with gages 7 and 8 start to diverge. The stiffener bays that contain gages 3 through 6 start to diverge at approximately 125 lbs/in. The predicted strains in the bay with strain gages 1 and 2 diverge at approximately 250 lbs/in.(not shown in Figure 24). A stiffener adjacent to the panel edge indicates some bending starting at approximately 25 lbs/in. as shown in Figure 25, otherwise all the other gages did not show any significantly unusual events. The results of two LVDT's measuring head displacement (panel end shortening) are shown in Figure 26. The dashed line shown with each curve is the linear least squares fit of the data from approximately 60 lbs/in. to the final load. The slope of these dashed lines would be the panel axial stiffness. The slopes of these lines are 373,795 lbs/in. and 362,577 lbs/in. with an average of 368,186 lbs/in., which would be the Panel #1 axial stiffness and is significantly higher than the analytical stiffness result. The out-of-plane deflections as indicated by LVDT's are shown in Figure 27. Three of the LVDT's are at the center of the panel length and one is at the quarter length point. The center of the panel (denoted by the filled circle) exhibits no noticeable out-of-plane displacement after a 50 lbs/in. load. The stiffener bays on either side of the center deflect in opposite directions as shown by the diamond and square symbols. The deflection at the quarter point (denoted by the filled triangle) is in the same direction as the centerline (square symbol).

Results from the moiré interferometry for the panel with an applied load of 200 lbs/in. are shown in Figures 28. Centerlines of the stiffener locations have been superimposed on the picture and the bays between the stiffeners have been numbered for reference. Comparing this full-field displacement (Figure 28) with the full-field displacement predictions in Figures 8b, 10, 13, 16 and 17 indicate that the experimental displacements do not match any of the predicted displacements in its entirety. The experimental results compare better with the linear analysis (Figures 8b, 10 and 16) than the nonlinear analysis. The displacements in bay 4 matched the analysis for model 2 (Figure 10). Bays 1, 2 and 3

could be considered a combination of the displacements from models 2 and 3.

Panel #2 - The strain results for the skin on Panel #2 are almost identical to the results for Panel #1 and are not shown here. The first and second stiffener from the panel edge indicate bending starting at initial loading of approximately the same magnitude as for Panel #1, otherwise all the other gages did not show any significant differences. The results from the two LVDT's measuring loading head displacement are shown in Figure 29. The dashed line shown with each curve is the linear least squares fit of the data from a load of approximately 60 lbs/in. to the final load. The slopes of the dashed lines shown in Figure 29 are 393,275 lbs/in. and 393,376 lbs/in. with an average of 393,325 lbs/in., which would be the axial stiffness for Panel #2. The out-of-plane deflections as indicated by LVDT's are shown in Figure 30. The center of the panel (denoted by the filled circle) exhibits no noticeable out-of-plane displacement after a 50 lbs/in. of applied load. The bays on either side of the panel center deflect in opposite directions as shown by the diamond and square symbols. The out-of-plane deflection magnitudes for Panel #2 (Figure 30) are in the opposite direction compared to Panel #1 deflections (Figure 27). The point at the panel quarter point for Panel #2 (denoted by the filled triangle) deflects in the same direction as the point at the centerline. Results from the moiré interferometry for a loads of 200 lbs/in. is shown in Figures 31. Comparing the full-field displacements also shows the reverse trend. The displacement of bay 4 of Panel #2 shown in Figure 31 is similar to the displacement pattern of bay 1 of Panel #1 (Figure 29).

A comparison of the analytical and experimental panel end-shortening results for the two panels are shown in Figure 32. The axial stiffness of the panels that were tested is nearly the same. Comparing the axial stiffness of the tested panel with the predicted stiffnesses indicates that the experimental stiffness values are 15 to 40 percent higher depending on model selected. Stiffness prediction from model 2 is the closest to the experimental stiffness value.

Shear Loading

The two panels that were evaluated in compression were then used for shear tests. The potting compound was removed from the ends of the specimens and the outer most two stiffener webs were removed to avoid interference with the fixture. A steel picture frame fixture was used where 21-inch square specimens can be tested. The shear test fixture was designed earlier using finite element analysis to minimize stress concentration effects (pinching/tearing) at the specimen corners and to ensure uniform shear loading in the panel.

The strain gages that were used during the compression tests (Figure 23) were also used to monitor strains during the shear tests. In addition, a dial gage was located at the center of one of the panels to measure out-of-plane displacements during tests. The specimens were tested successfully to 10,000 lbs (390 lbs/in., a postbuckling factor of 4.8) without any sign of failure. Up to that load, the stiffeners acted as panel breakers confining the skin buckling mode to the region between them. The tests were terminated at that point in order to save the specimens for subsequent tests with damage and/or for evaluation of fatigue loading response.

Strain data for two pairs of back-to-back strain gages are presented in Figure 33 and 34. The load at which the results from the back-to-back gages separate significantly from each other is an indication of a buckling event. Based on Figures 33 and 34 this load is approximately 90 lbs/in. This load value is in very good agreement with the predicted buckling load of 81.8 lbs/in. The computed strains at locations of strain gages 1 through 4 is also shown in Figures 33 and 34. In addition, the buckling mode was well predicted by the analysis. Model 2 was used for shear bucking analyses. A photograph of the buckled specimen under approximately 400 lbs/in. load is shown in Figure 35 which can be compared to the predicted shape from the finite element analysis shown in Figure 21. The out-of-plane displacement for the center of the specimen, for both panels are shown in Figure 36. The center of panel #1 did not move out-of-plane significantly until a load of approximately 200 lbs/in. (as shown in Figure 36) and then moved in the negative direction until loading was discontinued. The center of panel #2 started moving in the positive direction at buckling and this displacement continued to grow until approximately 300 lbs/in. and then reversed direction until the loading was discontinued. Also included on Figure 36 is the predicted out-of-plane displacement from the nonlinear analysis.

Conclusions

A design methodology has been presented for lightly-loaded post-buckled composite panels. A minimum weight and cost design of a typically loaded helicopter fuselage panel has been generated for applied loads of 120 lbs/in. in compression and 337 lbs/in. in shear. A finite element analysis of the

compression panels that included imperfections has been completed. Two test panels have been loaded in compression to 200 lbs/in., post-buckling factor of nearly two. The axial stiffness of the test panels were 15 to 40 percent higher, depending on the analysis model, than the predicted stiffness. The same panels were tested in shear. The finite element analysis of the shear panels predicted the buckling load within 10%. The buckling mode was also predicted very accurately for the shear load case.

References

1. Kassapoglou, C., and Dobyns, A.L. "Simultaneous Cost and Weight Minimization of Postbuckled Composite Panels Under Combined Compression and Shear," to appear in Structural and Multidisciplinary Optimization Journal, 2001.

2. Rankin, C. C., Brogan, F. A., Loden, W. A. and Cabiness, H. D., "STAGS Users Manual, Version 3.0," Lockheed Martin Missiles & Space Co., Inc., Advanced Technology Center, Report LNSC P032594, 1999.

3. Riks, E., "Progress in Collapse Analysis," Journal of Pressure Vessel Technology, Vol 109, 1987, pp. 27-41.

4. Park, K., C., "An Improved Stiffy Stable Method for Direct Integration of Nonlinear Structural Dynamics," Journal of Applied Mechanics, Vol. 42, June 1975, pp.464-470.

Table 1. Summary of material properties.

Property	Tape	Fabric
E_1 (Msi)	20.	9.8
E_2 (Msi)	1.31	9.8
$G_{12.}$(Msi)	0.62	0.64
μ_{12}	0.32	0.05
F_1^t (Ksi)	300.0	107.0
F_1^c (Ksi)	168.0	80.0
F_2^t (Ksi)	4.2	107.0
F_2^c (Ksi)	22.9	80.0
F_{12} (Ksi)	13.2	11.6

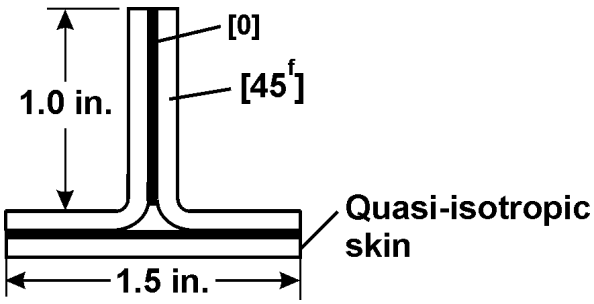

Figure 1. Stiffener configuration.

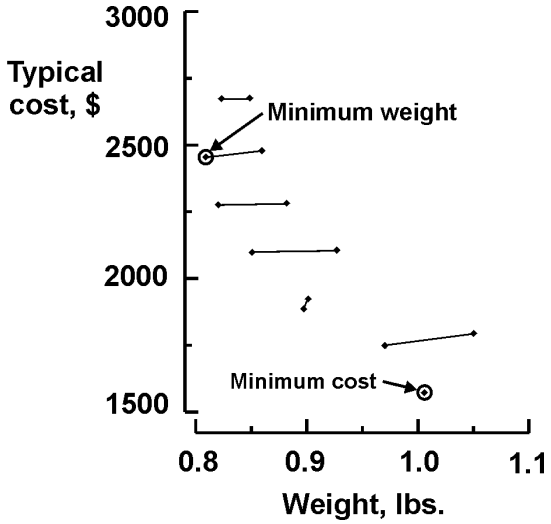

Figure 2. Panel cost as a function of weight.

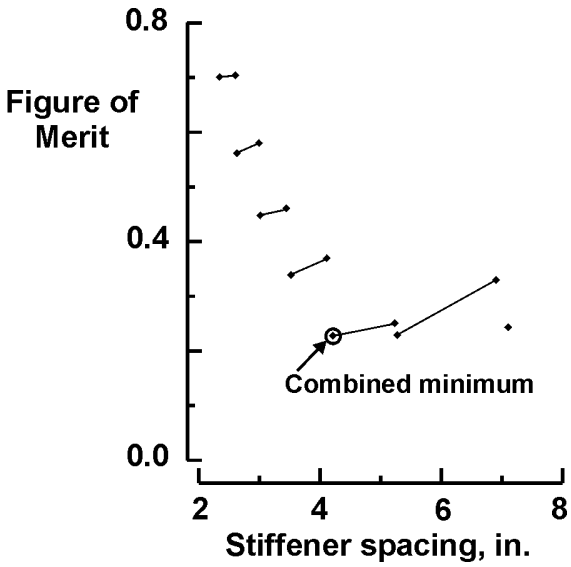

Figure 3. Figure of Merit as a function of stiffener spacing (combined cost and weight minimization).

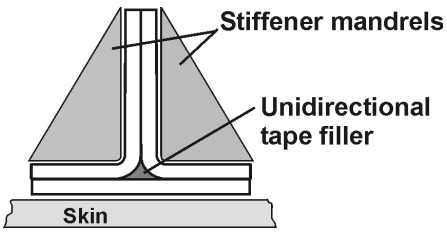

Figure 4. Stringer fabrication.

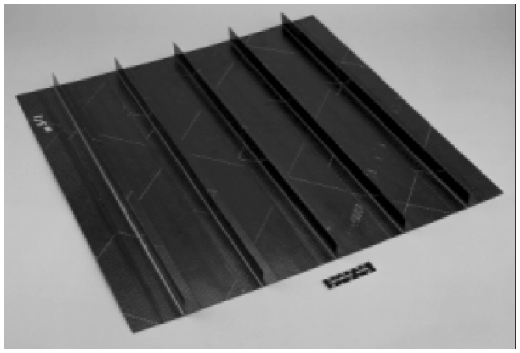

Figure 5. Photograph of I-stiffened panel.

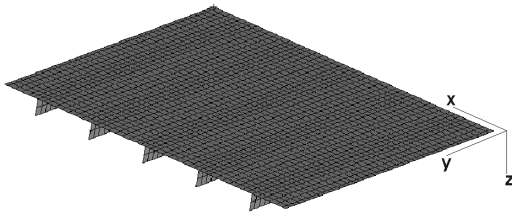

Figure 6. Finite element model of I-stiffened panel.

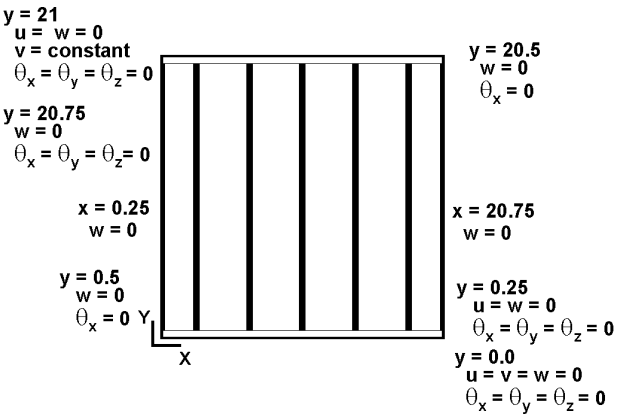

Figure 7. Boundary conditions for the finite element model.

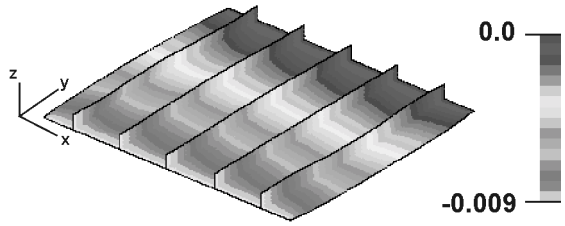

a. In-plane, v, displacements.

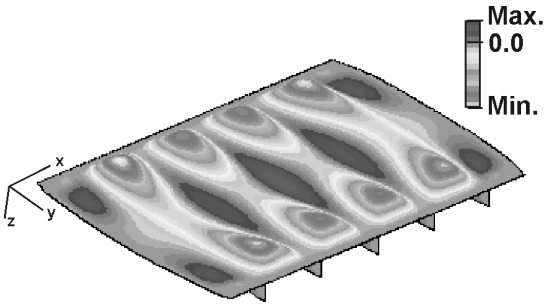

b. Out-of-plane, w. displacements

Figure 8. Predicted displacements for I-stiffened panel obtained using model 1.

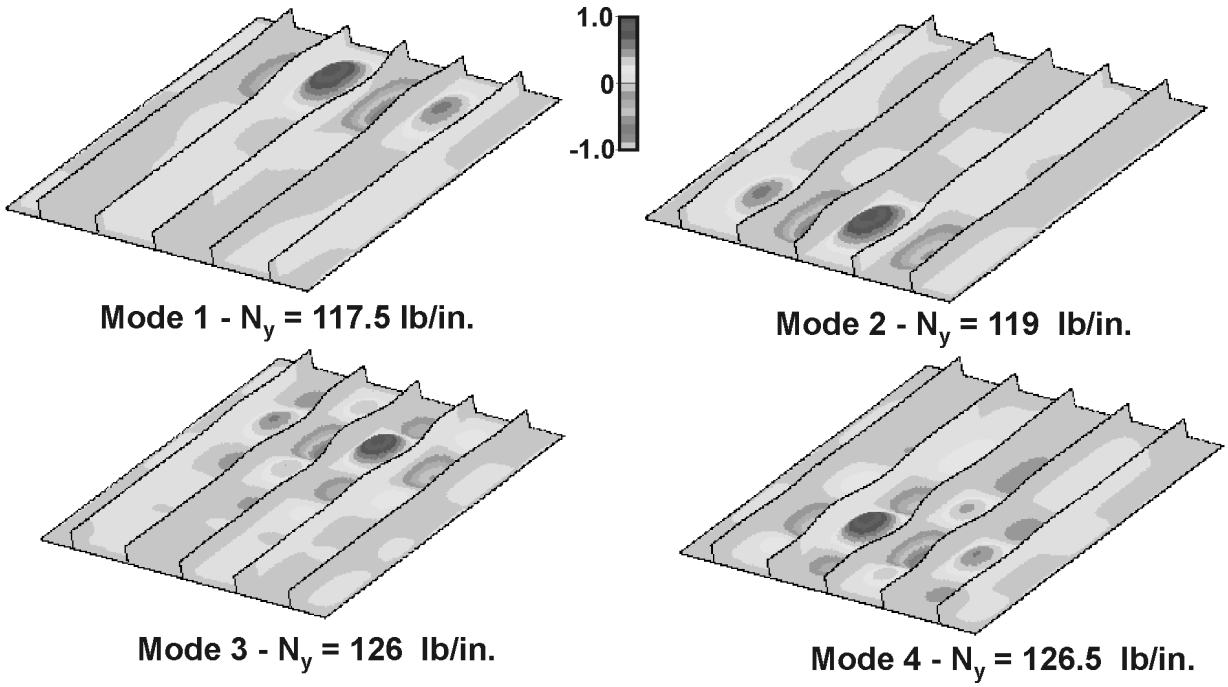

Figure 9. Predicted mode shapes and critical loads for the first four buckling modes from model 1.

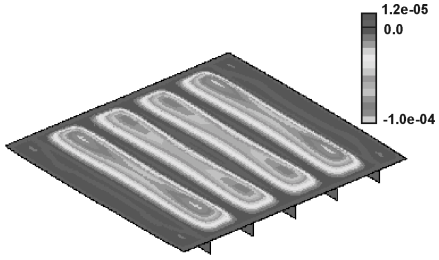

Figure 10. Out-of-plane displacements, w, from model 2 at ultimate load.

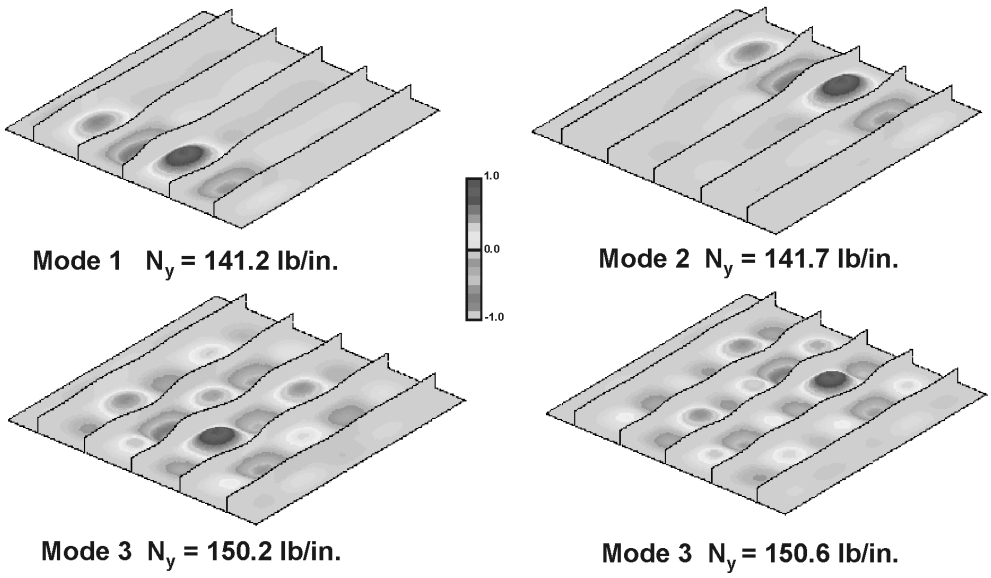

Figure 11. Predicted mode shapes and critical loads for the first four buckling modes from model 2.

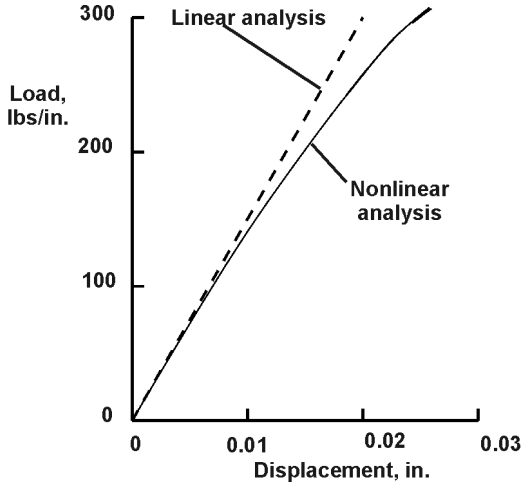

Figure 12. Panel end-shortening displacement as a function of load.

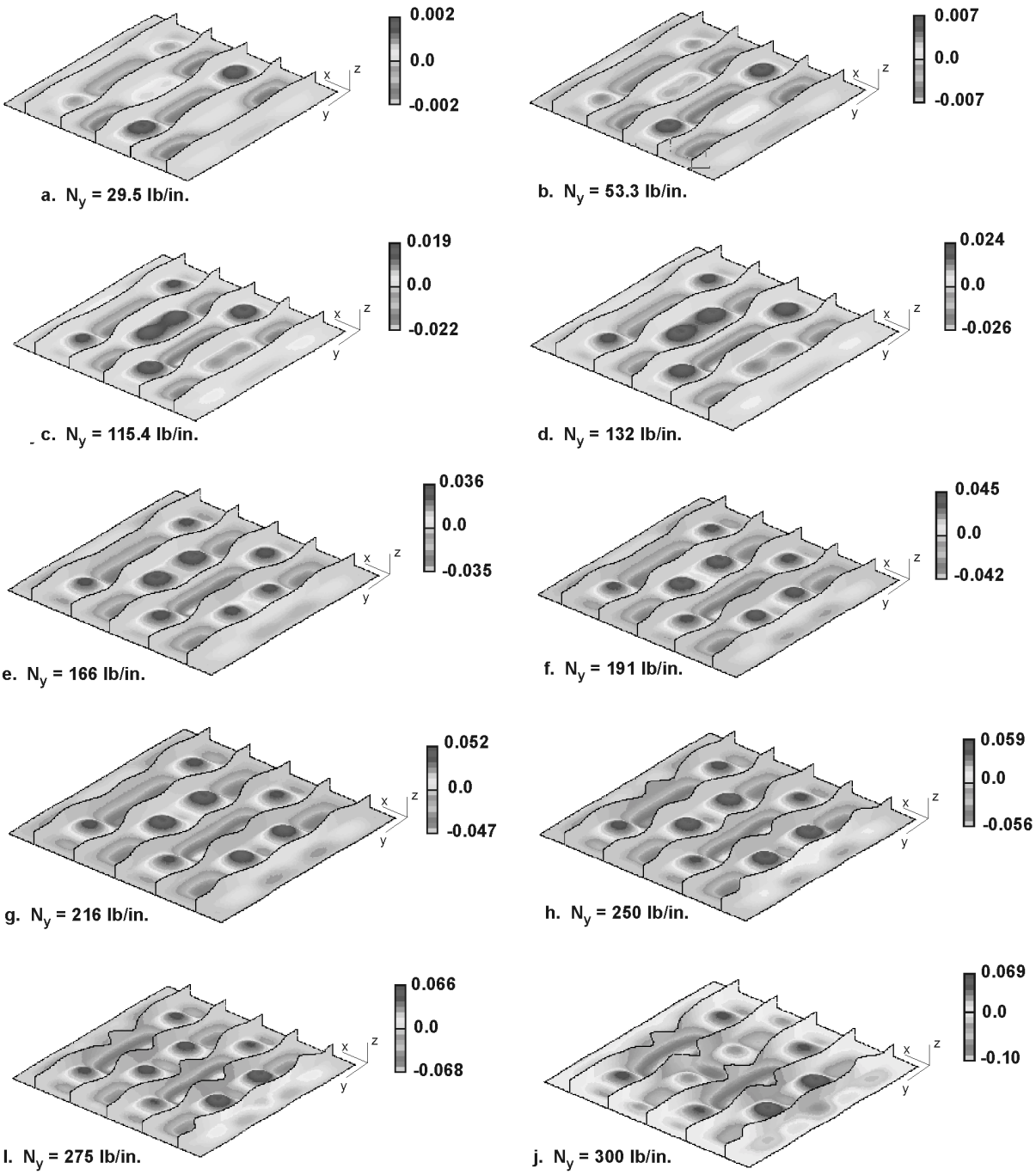

Figure 13. Predicted out-of-plane displacement contours from model 2 for different levels of applied loading.

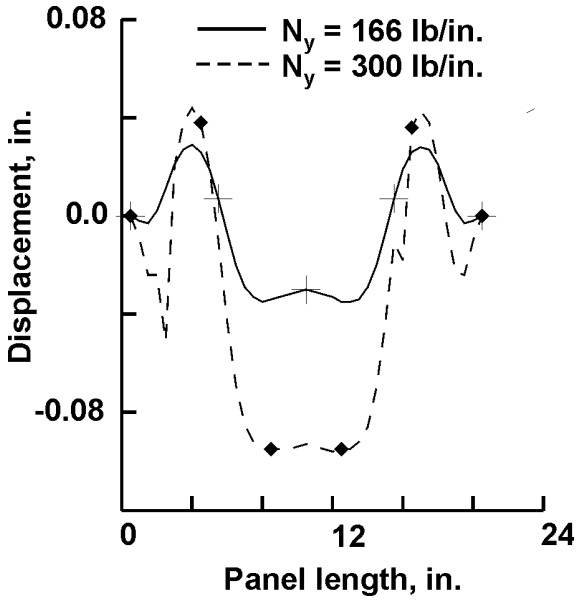

Figure 14. Predicted out-of-plane displacements along the panel length at a location 8.12 inches from the edge.

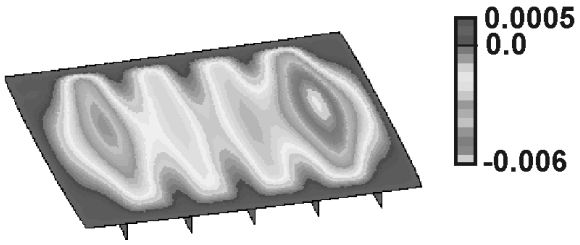

Figure 16. Predicted out-of-plane displacements for panel with imperfection.

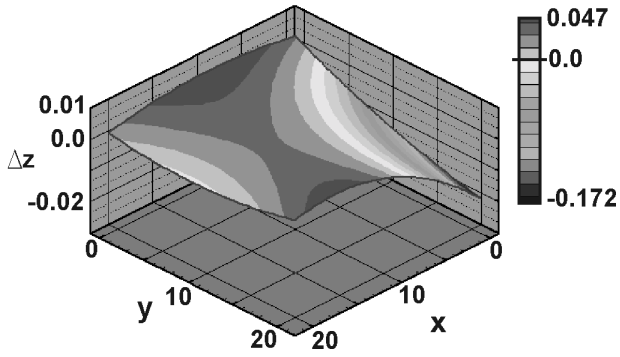

Figure 15. Deformed surface representing Panel #1.

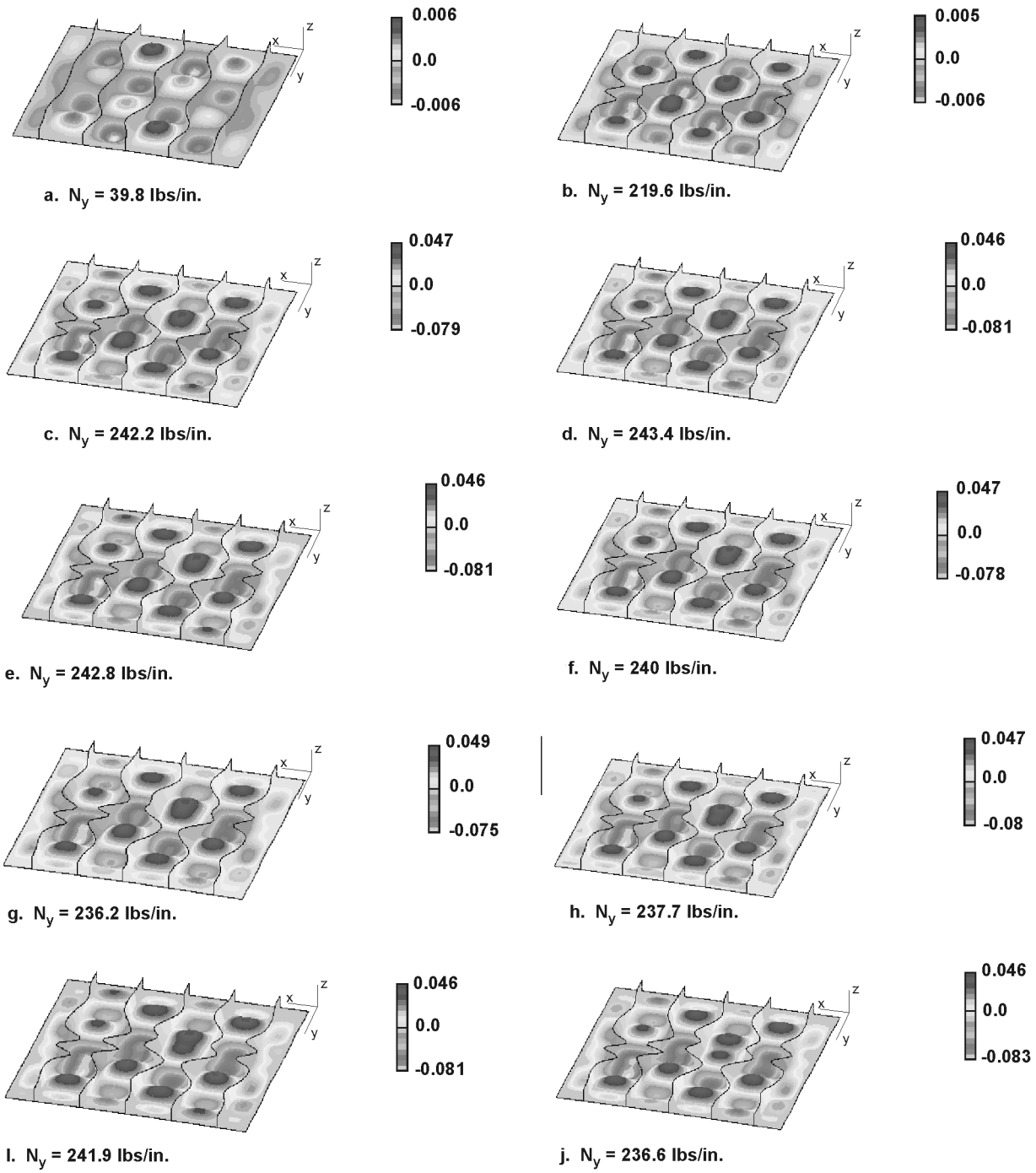

Figure 17. Predicted out-of-plane displacements at selected loads for model 3 with measured geometric imperfections.

Figure 18. Finite element model for shear panel analysis.

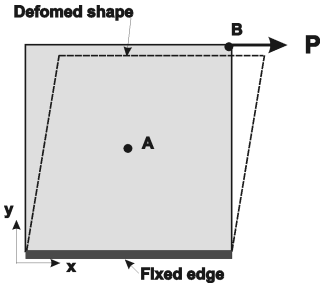

Figure 19. Shear panel model boundary conditions.

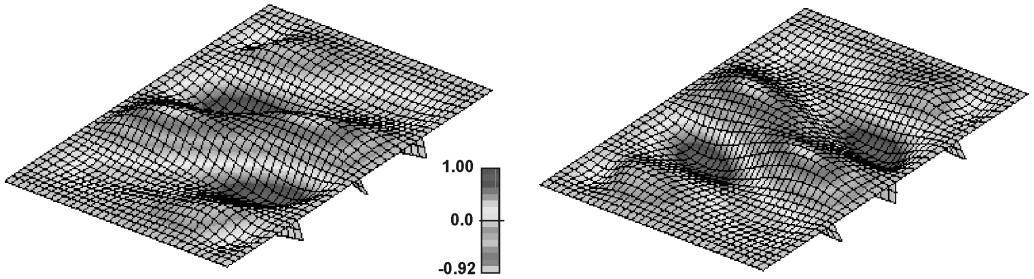

Figure 20. Predicted first and second buckling modes for shear loading.

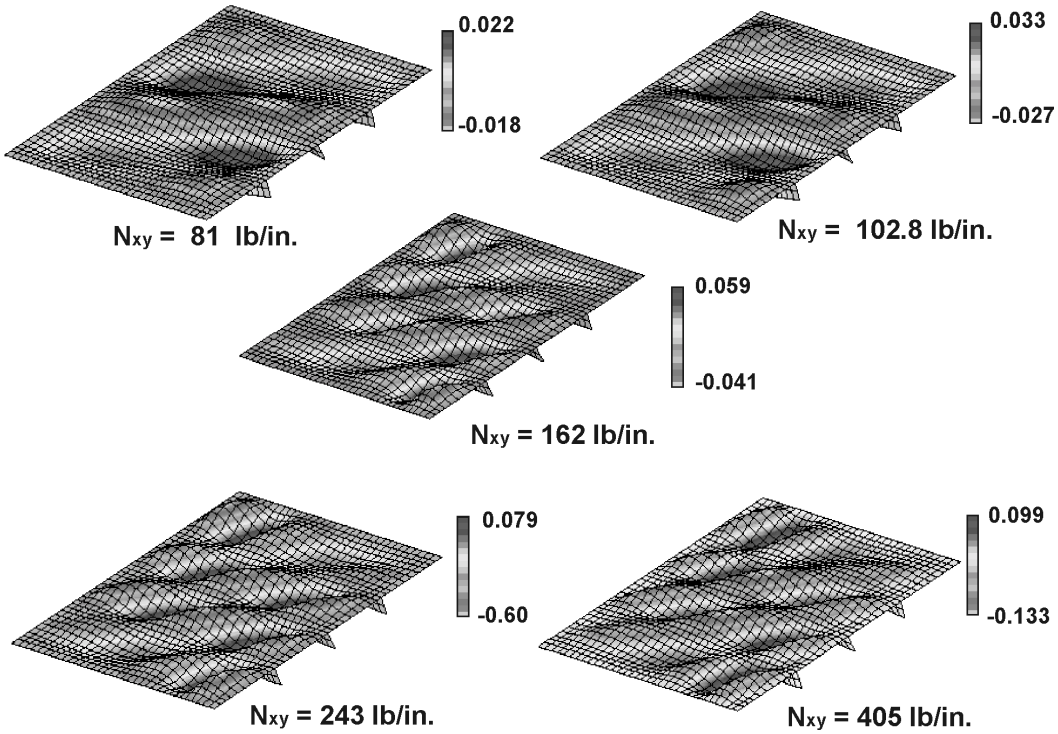

Figure 21. Predicted deflections from nonlinear analysis.

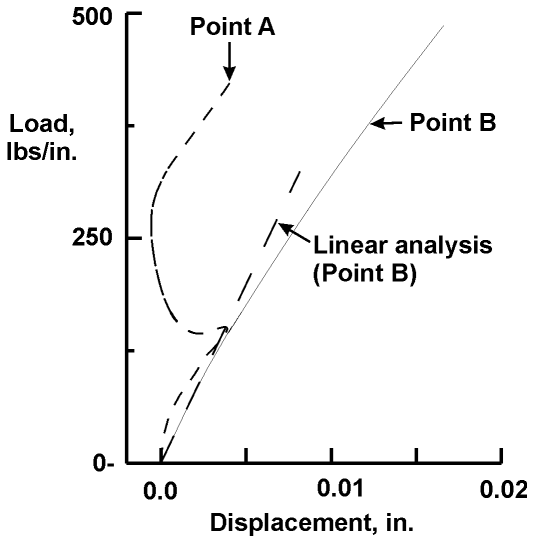

Figure 22. Predicted displacement at shear panel center and corner.

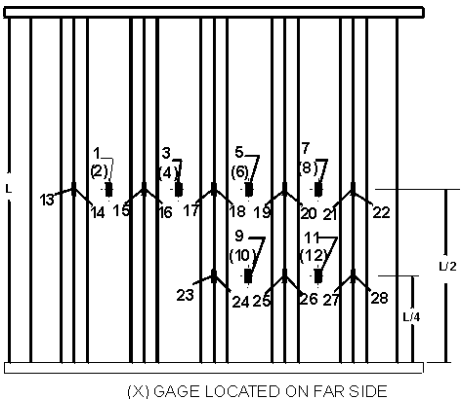

Figure 23. Strain gage locations.

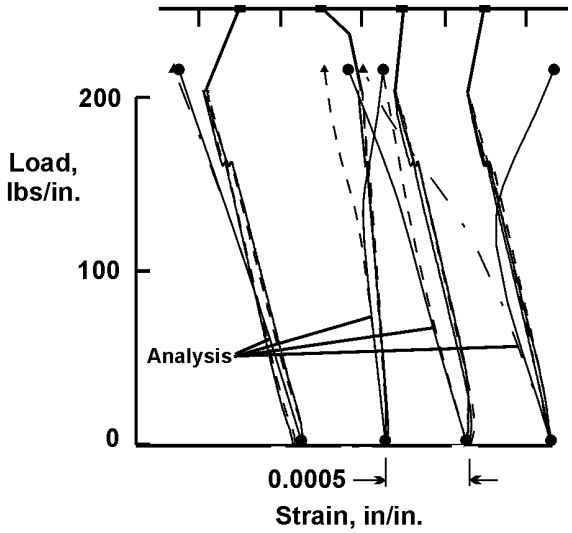

a. Strains across centerline, gages 1-8

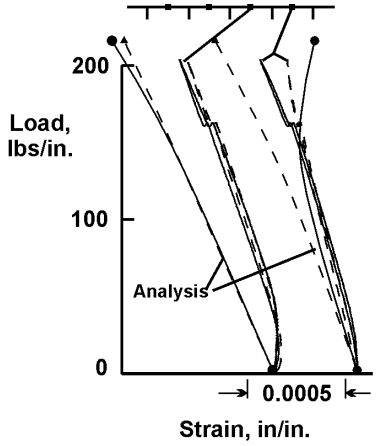

b. Strains at quarter point, gages 9-12

Figure 24. Strains in the skin of Panel #1.

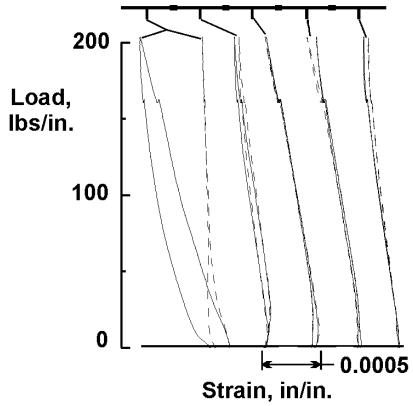

a. Strains at centerline, gages 13 – 22

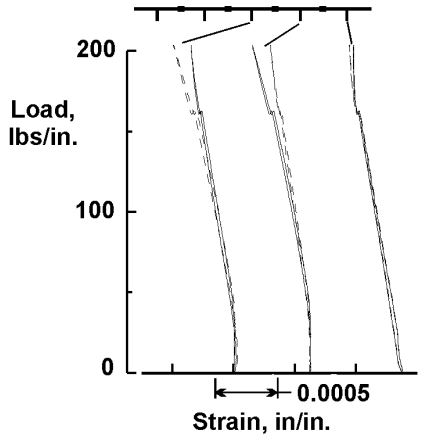

b. Strains at quarter point, gages, 23-28

Figure 25. Strains in the stiffeners of Panel #1.

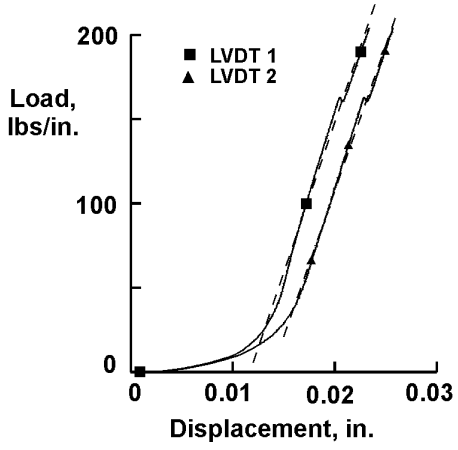

Figure 26. Panel #1 end-shortening displacement results.

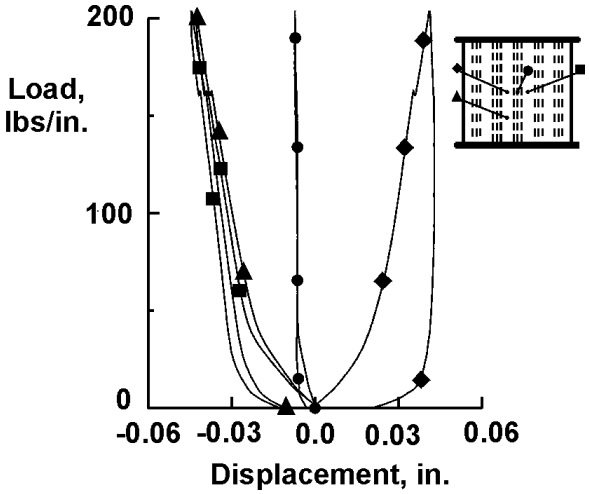

Figure 27. Out-of-plane displacement results for Panel #1.

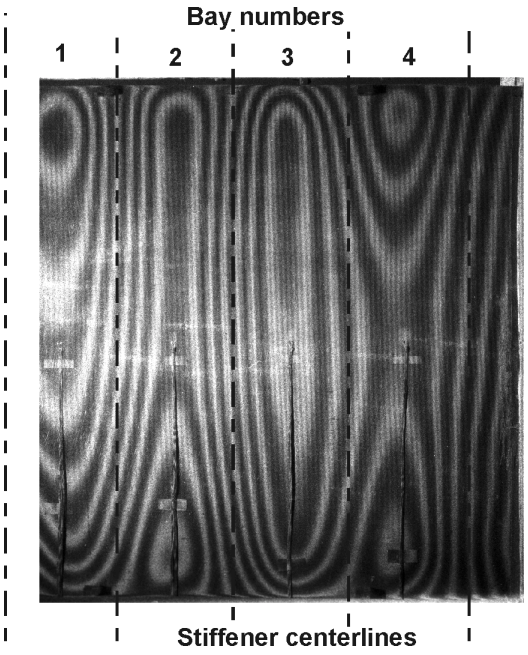

Figure 28. Moiré fringe pattern for Panel #1 at 200 lbs/in. of load.

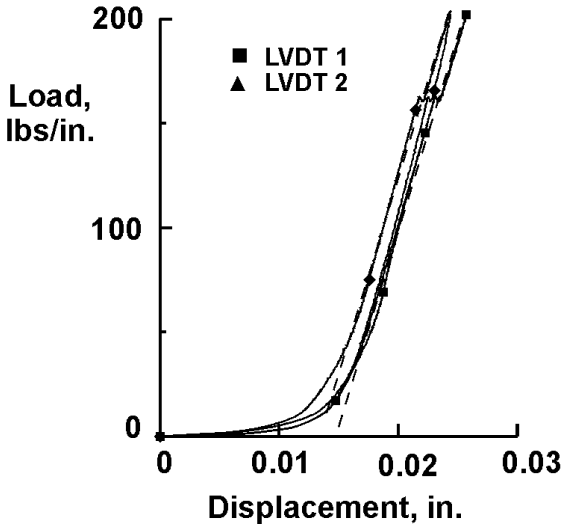

Figure 29. End-shortening displacement results

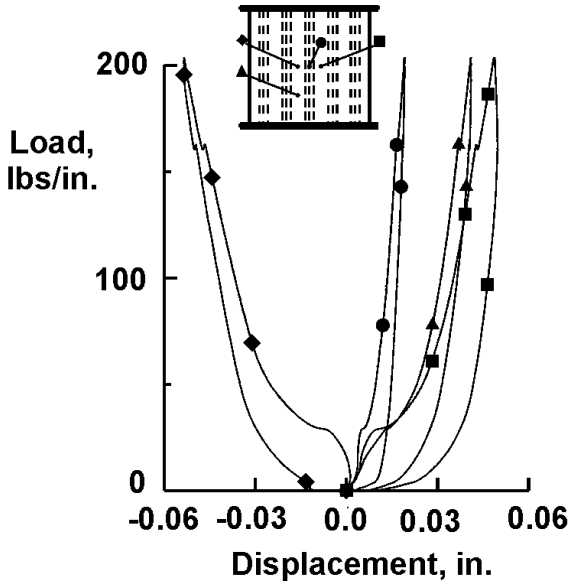

Figure 30. Out-of-plane deflections for Panel #2.

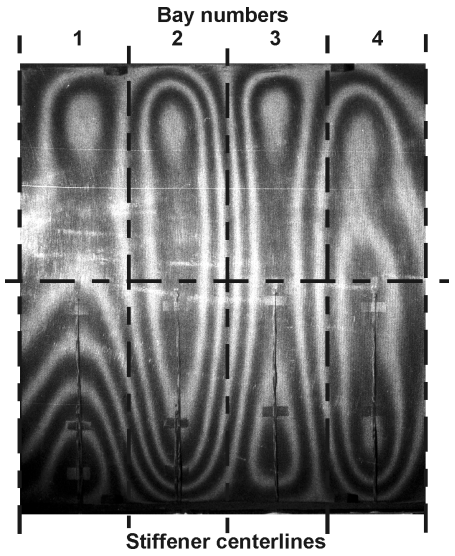

Figure 31. Moiré fringe pattern for Panel #2 at 200 lbs/in. load.

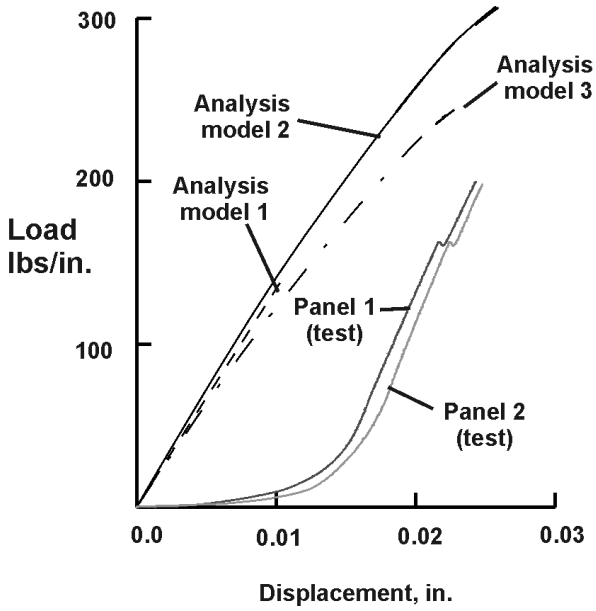

Figure 32. Comparison of analytical and experimental panel end-shortening results.

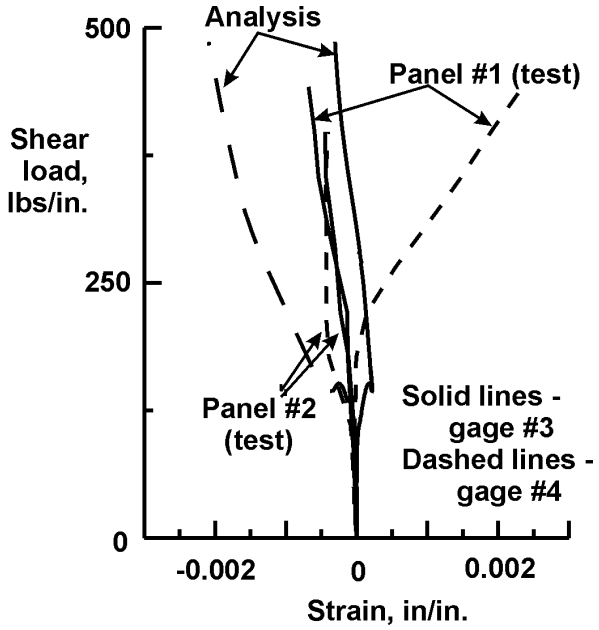

Figure 33. Comparison of results from strain gages #3 & #4 with analysis results.

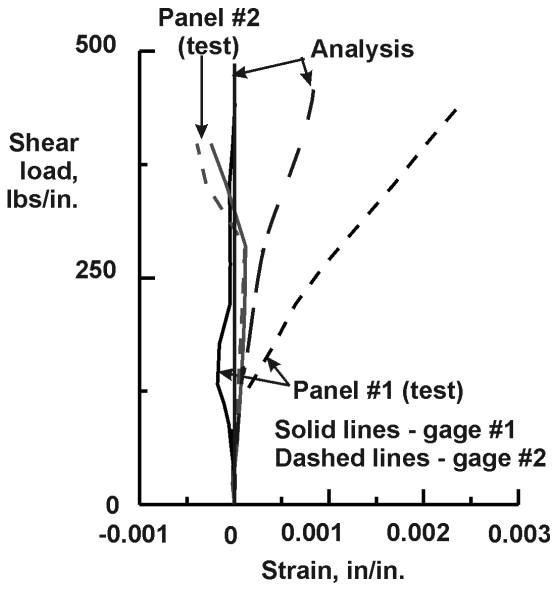

Figure 34. Comparison of results from strain gages #1 & #2 with analysis results.

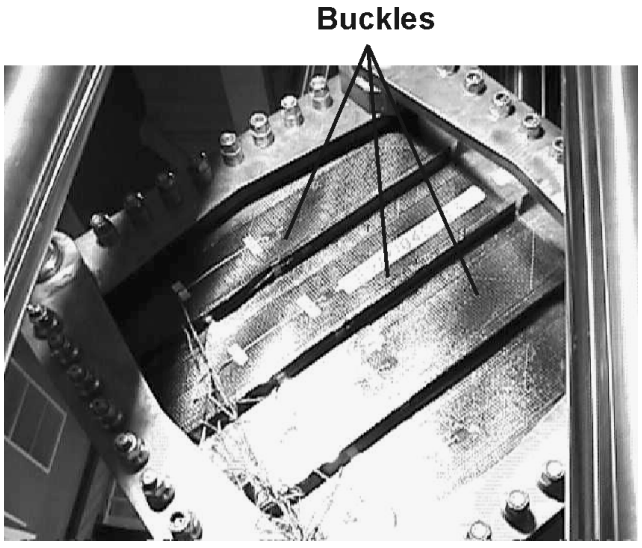

Figure 35. Photograph of shear panel with an applied load of 400 lbs/in.

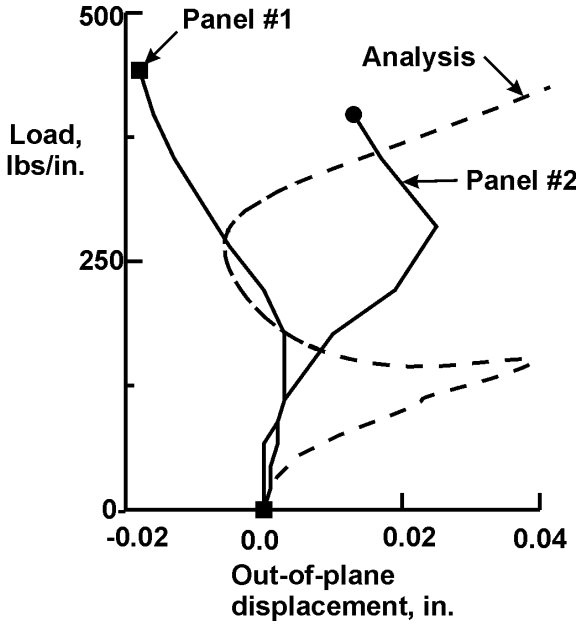

Figure 36. Comparison of out-of-plane displacements from test and analysis.